



**HAL**  
open science

## Goethite affects phytolith dissolution through clay particle aggregation and pH regulation

Zimin Li, Jean-Dominique Meunier, Bruno Delvaux

► **To cite this version:**

Zimin Li, Jean-Dominique Meunier, Bruno Delvaux. Goethite affects phytolith dissolution through clay particle aggregation and pH regulation. *Geochimica et Cosmochimica Acta*, 2023, 349, pp.11-22. 10.1016/j.gca.2023.03.021 . hal-04097659

**HAL Id: hal-04097659**

**<https://hal.science/hal-04097659>**

Submitted on 7 Jul 2023

**HAL** is a multi-disciplinary open access archive for the deposit and dissemination of scientific research documents, whether they are published or not. The documents may come from teaching and research institutions in France or abroad, or from public or private research centers.

L'archive ouverte pluridisciplinaire **HAL**, est destinée au dépôt et à la diffusion de documents scientifiques de niveau recherche, publiés ou non, émanant des établissements d'enseignement et de recherche français ou étrangers, des laboratoires publics ou privés.

1           **Goethite affects phytolith dissolution through clay particle aggregation and pH regulation**

2                                   Zimin Li<sup>a</sup>, Jean-Dominique Meunier<sup>b</sup>, Bruno Delvaux<sup>a</sup>

3  
4       <sup>a</sup> *Earth and Life Institute, Soil Science, Université catholique de Louvain (UCLouvain), Croix du Sud 2,*  
5                                   *L7.05.10, 1348 Louvain-La-Neuve, Belgium*

6       <sup>b</sup> *CNRS, CEREGE, Aix Marseille Université, IRD, INRAE, 13545 Aix-en-Provence Cedex 04, France*

7  
8       \*Corresponding author: zimin.li@uclouvain.be (Zimin Li)

9       Address: Earth and Life Institute, Soil sciences, Université catholique de Louvain (UCLouvain), Croix du  
10                   Sud 2 / L7.05.10, 1348 Louvain-la-Neuve, Belgium.

11  
12       Submitted to the journal *Geochimica et Cosmochimica Acta*

13       Tables: **3**

14       Figures: **8**

15       Pages: **21**

16       *Appendix A. Supplementary Material*

17 **Abstract**

18 Formed in plant tissues as fine silica particles, phytoliths are deposited within plant debris in soils where  
19 they can dissolve and feed silicon (Si) fluxes to the biosphere and hydrosphere. Yet, soil phytoliths can be  
20 protected from dissolution by entrapment in aggregates, and thus be withdrawn from the global silica cycle.  
21 Among clay-sized minerals interacting in stable aggregates, goethite and kaolinite are ubiquitous in soils.  
22 We analyzed the impact of goethite-mediated aggregation on the release of aqueous Si from phytoliths  
23 entrapped in microaggregates containing organic matter and kaolinite, with quartz and goethite at variable  
24 concentrations, simulating a soil sequence with increasing contents of clay and iron oxide, as it can  
25 commonly occur in terrestrial ecosystems. The microaggregates stored sizable amount of organic carbon,  
26 the release of which decreased with increasing goethite concentration. Aqueous Si was assessed through a  
27 kinetic extraction with dilute  $\text{CaCl}_2$ , while pH, aluminum (Al) and germanium (Ge) concentrations were  
28 measured in the  $\text{CaCl}_2$  extracts. Our experimental data showed that phytoliths were the source of aqueous  
29 Si. They also showed that the process of phytolith dissolution prevailed over Si adsorption on goethite. As  
30 mediated by goethite, aggregation protected phytoliths from dissolution at goethite concentrations above 20  
31  $\text{g kg}^{-1}$ . Increasing goethite concentration enhanced aggregation on the one hand, but increased pH from 5.5  
32 to 7.5 on the other. Thus, while aggregation significantly reduced the release of aqueous Si by 1.7- to 3-fold  
33 at a given pH, the increase in pH enhanced it. Overall, at common soil solution pH (5-6), aggregation  
34 reduced Si release by 2- 3 times. Thus, preservation of phytoliths in aggregates can be widespread in well-  
35 aerated soils and more effective than Si adsorption on secondary oxides in retaining Si.

36 **Keywords:** goethite, aggregation, phytolith preservation, dissolved silicon, low activity clays (LAC) soils.

## 37 **1. Introduction**

38 Since the pioneer quantitative study by Bartoli (1983), the role of plants in the terrestrial cycle of silicon (Si)  
39 has been largely documented (Derry et al., 2005; Meunier et al., 2022). The original source of dissolved Si  
40 (DSi) in soil is the reserve of weatherable silicate minerals (Garrels and Christ, 1965). Dissolved Si (DSi)  
41 is taken up as monosilicic acid ( $\text{H}_4\text{SiO}_4$ ) by plants where the mean Si concentration ranges between 1 and  
42  $100 \text{ g Si kg}^{-1}$  (Epstein, 1994; Hodson et al., 2005). In plant tissues, biogenic silica (BSi) precipitates as fine  
43 particles of opal-A ( $\text{SiO}_2 \cdot n\text{H}_2\text{O}$ ), named phytoliths, which return to soil within plant debris. Phytoliths are  
44 widespread in soils (Monger and Kelly, 2002) in which their content ranges from 1 to  $10 \text{ g kg}^{-1}$  worldwide,  
45 but may be higher locally (Meunier et al., 2014). Because of their relatively high dissolution rate (Frayse  
46 et al., 2009), phytoliths readily contribute to the reservoir of DSi, which can be (i) absorbed by plants and  
47 other biota (Puppe, 2020), (ii) sorbed by aluminum (Al) and iron (Fe) oxides (Bowden et al., 1973; Hiemstra  
48 et al., 2007; Haynes and Zou, 2020), (iii) precipitated into clay and/or silica minerals (Karathanasis, 2002),  
49 or (iv) leached and transferred to rivers and oceans (Bartoli, 1983; Derry et al., 2005). These processes  
50 impact the Si continent-ocean linkage, hence the global cycle of Si (Conley, 2002; Derry et al., 2005; Erhart,  
51 1963). Since Si is beneficial to plants (Coskun et al., 2019) while Si biological cycling is critical in primary  
52 productivity and C cycling on a global scale (Conley and Carey, 2015), Si plays a major role in the supply  
53 of numerous ecosystem services (Meunier et al., 2022). Therefore, understanding the mechanisms  
54 controlling DSi is a key issue. Among these mechanisms, the processes governing the resilience of  
55 phytoliths in soils are poorly known (Cornelis and Delvaux, 2016), despite recent advances showing that  
56 DSi release from phytoliths is also mediated by ageing (Liu et al., 2023, Puppe and Leue, 2018),  
57 microaggregation (Li et al., 2020; Li et al., 2022) and redox-dependent surface passivation (Koebernick et  
58 al., 2022). While the latter process requires alternating redox conditions (Koebernick et al., 2022) occurring  
59 in soils covering about 5-7% of global land surface (IUSS, 2015), microaggregation of soil particles is  
60 optimized in well-aerated soils with [clay + fine silt] content above 15%, in which biological activity  
61 enhances the formation of macro- and micro-aggregates (Oades, 1984; Six et al., 2004; Totsche et al., 2018).

62 Since well-aerated soils are, by far, largely dominant on earth (> 90% of global land surface), the impact of  
63 microaggregation on Si dynamics deserves a particular attention. An ample literature is available on the  
64 crucial role of microaggregates (< 250 $\mu$ m) on OC stabilization and turnover (Six et al., 2004; Totsche et al.  
65 2018). However, the role of microaggregates in soil functions and ecosystem services related to the cycling  
66 of other elements is poorly known (Totsche et al., 2018). About Si, phytoliths can be readily entrapped in  
67 microaggregates, as shown in long-term field experiments (Li et al., 2020) and short-term laboratory studies  
68 (Li et al., 2022). Aggregation reduced the release of DSi, strongly from microaggregates using allophane  
69 and ferrihydrite, but to a much lesser extent from microaggregates using kaolinite and goethite (Li et al.,  
70 2022). Allophane and ferrihydrite are only significant in some Andosols, which cover less than 1 percent of  
71 the global land surface, while crystalline mineral soils cover the majority of this surface (IUSS, 2015).  
72 Among these, soils with predominant kaolinite and goethite are widespread worldwide, since these minerals  
73 are ubiquitous (Bigam et al., 2002; White and Dixon, 2002). In particular, soils containing predominantly  
74 low activity clays (LACs), i.e., kaolinite and crystalline (Al, Fe) oxides, have a high potential to form stable  
75 aggregates at low organic matter (OM) content (Denef et al., 2002; Six et al., 2004) because kaolinite and  
76 (Al, Fe) oxides act as main binding agents (Denef et al., 2002), as does OM in permanent charge soils (Six  
77 et al., 2002). These LAC soils cover ~30% of the land surface at global scale and ~55% in the tropics (IUSS,  
78 2015; Sanchez, 2019). So far, the effect of crystalline oxide concentration on the release of DSi from  
79 microaggregates has not been evaluated.

80 Clay minerals, (Al, Fe) oxides and OM are the basic blocks of microaggregates, formed via cementing,  
81 which involve primarily physicochemical and chemical interactions, and gluing in which OM and microbial  
82 activity are crucial (Deng and Dixon, 2002; Totsche et al., 2018). Here, we focus on 1:1 clay – Fe oxide  
83 microaggregation which arises notably through binding oppositely charged surfaces of oxide and kaolinite  
84 (Schwertmann, 1988). Small amounts of Fe oxides promote microaggregation while their poor crystallinity  
85 and nano size enhance it (Schwertmann, 1988; Deng and Dixon, 2002; Totsche et al., 2018, Di Iorio et al.,  
86 2022; Guo et al., 2022). For crystalline oxides, conflicting observations were mainly attributed to the large

87 diversity of oxide crystal morphology and particle size (Schwertmann, 1988), but the impacts of oxide  
88 amount (see e.g., Di Iorio et al., 2022; Sanchez, 2019) and pH are still unclear. As kaolinite–oxide  
89 interactions are based on binding oppositely charged surfaces, increasing pH leads to surface charge change  
90 causing disaggregation (Bigham et al., 2002; Baalousha, 2009) or enhancing aggregation (Demangeat et al.,  
91 2018; Guo et al., 2002; Goldberg, 1989), likely depending on OM content (Baalousha et al., 2008).

92 Here, we analyzed the role of goethite-mediated aggregation in releasing DSi from phytoliths by testing two  
93 hypotheses. (i) Aggregation-induced protection of phytoliths and delayed dissolution occur at low goethite  
94 concentrations. (ii) pH change affects aggregation, thus phytolith protection and DSi release. We used  
95 aggregates incubated from mixtures made of phytoliths, OM and kaolinite in fixed proportions, quartz and  
96 goethite in variable proportions. We quantified the release of DSi as impacted by aggregation and pH, and  
97 traced its source using the geochemical proxies Ge/Si and Al/Si molar ratios.

98

## 99 **2. Materials and methods**

### 100 **2.1. Individual components**

101 *Phytoliths* were extracted from rice plant (*Oryza sativa indica* IR64; IRRI) leaves (Li et al., 2019; Li et al.,  
102 2022), purified (Kelly, 1990), washed and oven-dried at 50 °C (Li et al., 2022). *Quartz* was supplied by  
103 Merck KGaA Co, Darmstadt, Germany, the particles being of calibrated size 330–500 µm. *Organic matter*  
104 (OM) was oven-dried at 45 °C and finely ground Egyptian clover (*Trifolium alexandrinum*). Charentes  
105 *kaolinite* (Cases et al. 1982; Cases et al., 2000; Delineau et al., 1994; Yvon et al., 1982) contained minor  
106 amounts of Fe ( $\text{Si}_2\text{Al}_{2-x}\text{Fe}_x\text{O}_5(\text{OH})_4$ ,  $x \leq 0.02$ ) (Mestdagh et al., 1982). *Goethite* was synthesized after  
107 adding 5 M NaOH (70 ml) to 1 M  $\text{Fe}(\text{NO}_3)_3$  (100 ml) under intense stirring and brought to pH > 12, washing  
108 and drying (Cornell and Schwertmann, 1996). As reported earlier (Li et al., 2022), the constituents exhibited  
109 characteristic morphologies and X-ray diffraction patterns as well as specific surface area (SSA), which  
110 decreased in the sequence ( $\text{m}^2 \text{g}^{-1}$ ): phytoliths (190) > goethite (132) > kaolinite (24) > quartz (1). Besides,

111 in the pH range 4.5-7.5, kaolinite and OM carried a negative surface charge while goethite carried a positive  
112 surface charge as predicted from its pH value at the isoelectric point ( $\text{pH}_{\text{IEP}} = 9.6$ , Li et al., 2022).

## 113 **2.2. Mixtures and aggregates**

114 The individual components were mixed to prepare bulk mixtures using fixed concentrations of ( $\text{g kg}^{-1}$ ): rice  
115 phytoliths (20), OM (50), kaolinite (370), and variable concentrations of goethite and quartz, with the  
116 goethite concentration increasing from 0 to  $80 \text{ g kg}^{-1}$  while correspondingly decreasing the quartz content  
117 from 560 to  $420 \text{ g kg}^{-1}$ . Since both goethite and kaolinite used here are clay-sized, these assemblages  
118 simulate a pedological continuum of LAC soils for which clay content increases from 370 to  $450 \text{ g kg}^{-1}$  with  
119 the increase in Fe oxide concentration as can commonly occur in intertropical regions (Sanchez, 2019; Van  
120 Wambeke, 1992). The bulk mixtures were divided into two parts, designed as *mixtures* and *aggregates*, both  
121 in triplicate. The *mixtures* were in fact the initial bulk mixtures, just juxtaposing the individual components,  
122 not subjected to watering and ageing. The *aggregates* were produced from bulk mixtures that were irrigated  
123 with deionized water using a liquid/solid ratio 0.6/1.0  $\text{g g}^{-1}$ , incubated in darkness at  $20^\circ\text{C}$  for 32 days, and  
124 freeze-dried (Filimonova et al., 2016). In fact, Filimonova et al. (2016) observed well developed  
125 microaggregates after 20 days, but with allophane, ferrihydrite and OM. We extended the incubation to 32  
126 days in order to consider the appropriate aggregate formation times as previously estimated for soils with  
127 OM and crystalline minerals (Chenu and Cosentino, 2011; De Gryze et al., 2006; Segoli et al., 2013; Totsche  
128 et al., 2018). Our aggregates were then gently grinded and sieved at 2 mm. For easy reading, mixtures and  
129 aggregates will be designated by their goethite concentration: mixture-X and aggregate-X where  $X = 0, 10,$   
130  $20, 40, 60$  or  $80 \text{ g kg}^{-1}$ .

## 131 **2.3. Microscopic investigations**

132 Scanning electron microscopy (SEM) was performed on aggregates ( $< 2 \text{ mm}$ ) without any chemical  
133 pretreatment using a field emission gun SEM (FEG-SEM; Zeiss Ultra55), equipped with an EDX system  
134 (Jeol JSM2300 with a resolution  $<129 \text{ eV}$ ) to assess the micro-scale distribution of elements: carbon (C),  
135 oxygen (O), Fe, Al, and Si. Aggregates were also visualized by Transmission Electron Microscopy (TEM)

136 on samples sieved at 250  $\mu\text{m}$ , using a LEO 922 Omega Energy Filter Transmission Electron Microscope  
137 operating at 120 kV.

## 138 **2.4. Chemical analyses**

139 *Elemental analysis.* Elemental analyses (Table 1) confirmed the expected value of the Al/Si ratio for  
140 kaolinite (1.01 mol mol<sup>-1</sup>) while the Ge/Si decreased in the order ( $\mu\text{mol mol}^{-1}$ ): kaolinite (4.37) > quartz  
141 (2.10) > phytoliths (0.41). In this study, the total concentrations of Si, Al and Ge were measured in triplicate  
142 in the mixtures and aggregates. They were determined by Inductively Coupled Plasma - Atomic Emission  
143 Spectrometry (ICP–AES, Jarrell Ash Iris Advantage) after calcination at 500°C for 24h, fusion in Li-  
144 metaborate + Li-tetraborate at 1000 °C (Chao and Sanzolone, 1992), and then ash dissolution with a diluted  
145 10% HNO<sub>3</sub> solution. Germanium (Ge) concentration was measured by ICP Mass Spectrometry (ICP-MS)  
146 in powder samples (100 mg) after alkaline fusion using sodium peroxide (Na<sub>2</sub>O<sub>2</sub>) in a glassy carbon crucible,  
147 heating to 600–800 °C until reaction ceased, and dissolution of the residual vitreous mass with a diluted 2%  
148 HNO<sub>3</sub> solution (500ml). Accuracy and long-term repeatability of Ge analysis were well assessed. The  
149 detection limit was  $0.8 \times 10^{-3}$  ppb. The analytical measurement precision was  $\pm 2\%$ . The BHVO-2 standard  
150 (basalt rock powder) was systematically dosed every two samples in each analytical series. The C and N  
151 concentrations were measured by a Flash 2000 Elemental Analyzer (Thermo Fisher Scientific, Waltham,  
152 MA, USA).

153 *Specific extractions from individual components, mixtures and aggregates.* The Na<sub>2</sub>CO<sub>3</sub>- and CaCl<sub>2</sub>-  
154 extractable Si and Al concentrations were determined through kinetic extractions in triplicate to assess the  
155 contents of BSi or amorphous Si (ASi) (DeMaster, 1981; Koning et al., 2002; Saccone et al., 2006) and  
156 aqueous or bioavailable Si (Haysom and Chapman, 1975; Sauer et al., 2006), respectively. As for elemental  
157 analyses, the Na<sub>2</sub>CO<sub>3</sub> extraction was not repeated here for the individual components since their Na<sub>2</sub>CO<sub>3</sub>  
158 extractable Si and Al contents were already discussed by Li et al. (2022). However, the CaCl<sub>2</sub> extraction  
159 was repeated here for the individual components and performed simultaneously with the mixtures and  
160 aggregates for comparison purposes under identical experimental conditions of temperature, pressure and

161 ionic strength. *Na<sub>2</sub>CO<sub>3</sub> extraction.* Thirty mg of sample (mixture, aggregate) was mixed in 40ml of Na<sub>2</sub>CO<sub>3</sub>  
162 0.1M, pH = 11.2, and digested for 5 h at 85 °C. One ml of extraction solution was collected at 1, 2, 3, 4 and  
163 5 h, then neutralized and acidified by adding 100 µl of 7M HNO<sub>3</sub> to analyze dissolved Si and Al using ICP–  
164 AES. The time evolutions of extracted Si and Al (Na<sub>2</sub>CO<sub>3</sub>-Si and -Al) were used to estimate the pools of  
165 ASi and amorphous Al (AAI) as described in Li et al. (2022). *CaCl<sub>2</sub> extraction.* As mentioned above, we  
166 carried out the CaCl<sub>2</sub> extractions for the individual components, mixtures and aggregates to produce  
167 experimental data in strictly identical conditions. Instead of using standard protocols, we carried out a  
168 prolonged (64d) kinetic extraction (Li et al., 2019) for the individual components, mixtures and aggregates  
169 using a solid:liquid ratio 2g:20ml (unbuffered 0.01M CaCl<sub>2</sub>) in a plastic centrifuge tube through  
170 continuously shaking under darkness at 20 °C. The CaCl<sub>2</sub> extractant was unbuffered since buffering agents  
171 readily interact with components and interfere in colloidal interactions. Adjusting pH by adding acid or base  
172 can also impact the release of Si by mineral or phytolith dissolution. The 2:20 solid:liquid ratio was kept  
173 constant using replicates for both the extraction and analysis. At each time step (16h, 2, 4, 8, 16, 32 and 64  
174 days), the collected suspension (20 ml) was centrifuged at 3,000g for 20 min. The supernatant (15ml) was  
175 filtered and separated in two aliquots to measure pH (5 ml) and solutes concentrations (10ml). The latter  
176 extract was separated in two aliquots of 5 ml to determine, as described above, Si and Al concentration by  
177 ICP-AES and Ge concentration by ICP-MS, respectively, at each kinetic step. Each 5-ml aliquot was diluted  
178 with Milli-Q water by 10 times before assaying Si and Al, but by 2.5 times before dosing Ge. In both cases,  
179 each 5 ml aliquot was acidified by adding 50 µl 7M HNO<sub>3</sub>. These determinations were aimed to quantify  
180 the release of aqueous Si as well as to trace its origin using the Al/Si and Ge/Si molar ratios. Following  
181 Houba et al. (2000), we measured dissolved OC (DOC) in the 0.01M CaCl<sub>2</sub> extract at 16h with a TOC  
182 analyzer (TOC-L, CPN; Shimadzu).

183

### 184 **3. Results**

#### 185 **3.1. Characteristics of the materials**

186 Table 1 showed, as expected, the decrease in Si and Ge concentrations in the aggregates with the increase  
187 in their goethite content. Concomitantly, the Al/Si ratio increased from 0.22 to 0.26, while the Ge/Si ratio  
188 remained unchanged (2.5-2.6). The SEM images showed phytolith particles embedded in aggregate matrix  
189 (Fig. 1a-e), with the typical bilobate shape of rice phytoliths (ICPT, 2019; Zuo et al., 2017) associated with  
190 highest contents of Si and O (Fig. 1a-e). The SEM-EDX data also showed a very close interlocking of the  
191 different components within fine-sized microaggregates ( $< 250 \mu\text{m}$ ), making it difficult to target individual  
192 constituents for detecting their respective chemical compositions (Table 1). As expected, the normalized  
193 mass percent of Fe increased with increasing goethite loading. The TEM micrographs illustrated intimate  
194 associations of fine clay-sized kaolinite and goethite (Fig. 1g-j). Fig. 1k (see also Table S1) showed that  
195 DOC release from mixtures and aggregates decreased with increasing goethite content, while for a given  
196 goethite concentration, DOC was significantly lower in the aggregate relatively to the unaggregated mixture.

197 **3.2.  $\text{Na}_2\text{CO}_3$  extractable Si and Al.**  $\text{Na}_2\text{CO}_3$ -Al was not detected in phytoliths, while both  $\text{Na}_2\text{CO}_3$ -Al and  
198  $\text{Na}_2\text{CO}_3$ -Si were not detected in quartz and OM (Fig. S3 in Li et al., 2022). The contents of amorphous Si  
199 (ASi) and Al (AAI) (Table 2) were estimated from the time evolution of  $\text{Na}_2\text{CO}_3$ -Si and  $\text{Na}_2\text{CO}_3$ -Al for  
200 mixtures and aggregates (Fig. S1). Largely differing between phytoliths and kaolinite (272 vs  $1.2 \text{ g kg}^{-1}$ ),  
201 the concentration of ASi varied from 5.9 to  $9.2 \text{ g kg}^{-1}$  in unaggregated mixtures, where it increased with  
202 goethite content, and between 6 and  $6.8 \text{ g kg}^{-1}$  in the aggregates. The ASi content significantly differed  
203 between mixtures and aggregates only in the absence of goethite and at goethite concentration of 60 and 80  
204  $\text{g kg}^{-1}$ . The AAI/AASi molar ratio was close to unity for kaolinite, but was largely below 1 for the mixtures  
205 (0.05-0.125) and aggregates (0.018-0.045). Clearly, the increase in goethite content in the mixtures (not  
206 shown) and aggregates (Table 2) led to the concomitant decrease in total Si and Ge concentrations, thus  
207 giving a Al/Si ratio increasing from 0.22 to  $0.26 \text{ mol mol}^{-1}$  and Ge/Si ratio remaining unchanged (2.5-2.6  
208  $\mu\text{mol mol}^{-1}$ ). The Ge/Si ( $\text{mmol mol}^{-1}$ ) values for phytoliths (0.41) and kaolinite (4.36) were in agreement  
209 with data reported in the literature (Li et al., 2022, and references therein). The respective Al, Si and Ge  
210 concentrations in kaolinite, phytoliths and quartz were used to compute the aggregate Al/Si and Ge/Si ratios,

211 which ranged from 0.23 to 0.26 mol mol<sup>-1</sup> (Al/Si) and from 2.5 to 2.6 μmol mol<sup>-1</sup> (Ge/Si), in agreement with  
212 measured values (Table 1).

### 213 3.3. CaCl<sub>2</sub> extractable Si, Al and Ge, and pH

214 The pH of the CaCl<sub>2</sub> extract (pH<sub>CaCl<sub>2</sub></sub>) ranged between 3.5 and 3.9 for kaolinite, decreased with increasing  
215 extraction time from 5.8 to 4.4 for quartz, and from 4.3 to 3.5 for phytoliths (Fig. S2, Table S2). As shown  
216 in Fig. 2 (values in Table S2), pH<sub>CaCl<sub>2</sub></sub> increased with increasing time for all mixtures from 4.9-5.1 after 16h  
217 to 5.5-7.5 after 64d (Fig. 2, Table S2). At 16h timestep, pH<sub>CaCl<sub>2</sub></sub> values (4.9-5.1, Table S2) did not  
218 significantly differ between goethite loadings. However, at 64d, they significantly differ by 2 pH units, this  
219 difference being related to the goethite concentration in the mixture. At 64d, the pH<sub>CaCl<sub>2</sub></sub> value indeed  
220 increased from 5.5 to 7.5 with the increase in goethite content from 0 to 80 g kg<sup>-1</sup>. In contrast, for the  
221 aggregates, the range of pH<sub>CaCl<sub>2</sub></sub> was two pH units after 16h (5.2-7.2) but narrower after 64d (7.2-7.9) without  
222 dependence on goethite concentration (Fig. 2).

223 As observed by Li et al. (2022), Si and Al were not detected here in the CaCl<sub>2</sub> extract for OM. Same as Li  
224 et al. (2022), the concentration of Si in the CaCl<sub>2</sub> extract (CaCl<sub>2</sub>-Si) decreased in the order (g kg<sup>-1</sup>, 16h-64d):  
225 phytoliths (0.2–5.6) > kaolinite (0.01–0.15) > quartz (0.001-0.02) (Fig. S2) while CaCl<sub>2</sub>-Al was not detected  
226 for phytoliths and quartz. For kaolinite, CaCl<sub>2</sub>-Al increased from 0.9 to 0.5 × 10<sup>-6</sup> mol l<sup>-1</sup> with increasing  
227 extraction time (Table S2), giving a Al/Si ratio decreasing from 1.1 to 0.15 (Fig. S2). The kinetic curves  
228 showed the release of CaCl<sub>2</sub>-Si from the unaggregated mixtures and aggregates in Fig. 3. In the former (Fig.  
229 3a), CaCl<sub>2</sub>-Si increased to a value at 64d depending on the goethite concentration in the mixture, as CaCl<sub>2</sub>-  
230 Si at 64d increased from 335 to 575 mg Si kg<sup>-1</sup> with increasing goethite content. In contrast, the range of  
231 CaCl<sub>2</sub>-Si at 64d was narrower in the aggregates as it varied from 395 to 430 mg Si kg<sup>-1</sup>, with no dependency  
232 on goethite content (Fig. 3b). At goethite concentrations above 20 g kg<sup>-1</sup>, CaCl<sub>2</sub>-Si at 64d was significantly  
233 lower in the aggregates than in the mixtures (Fig. 3c). The range of Al concentration in the CaCl<sub>2</sub> extracts  
234 (CaCl<sub>2</sub>-Al) was 1.4 × 10<sup>-6</sup>–1.9 × 10<sup>-4</sup> mol l<sup>-1</sup> in the mixtures and 0.8 × 10<sup>-6</sup>–1.0 × 10<sup>-4</sup> mol l<sup>-1</sup> in the  
235 aggregates (Table S2) with no specific trend along increasing extraction time (Fig. S3).

236 For both the mixtures and aggregates (Fig. 4), the Ge concentration in the CaCl<sub>2</sub> extract (CaCl<sub>2</sub>-Ge)  
237 systematically reached a maximum value at 32d. Yet, the time evolution of CaCl<sub>2</sub>-Ge exhibited distinct  
238 patterns between mixtures and aggregates. In the mixtures, the range of CaCl<sub>2</sub>-Ge ( $\mu\text{mol kg}^{-1}$ ) was 0.51-  
239 1.08 at 16h and 0.06-2.12 at 64d closely depending on the goethite concentration (Fig. 4a), whereas in the  
240 aggregates, the range of CaCl<sub>2</sub>-Ge ( $\mu\text{mol kg}^{-1}$ ) was 0.29-0.71 at 16h and 0.11-0.61 at 64d with no  
241 dependency on goethite content (Fig. 4b). As shown in Fig. 4c-d, the lower release of Ge in CaCl<sub>2</sub> in the  
242 aggregates was significant at 16h and 64d at goethite concentration  $\geq 10 \text{ g kg}^{-1}$ , but the reduction of CaCl<sub>2</sub>-  
243 Ge after aggregation was much larger at the highest goethite contents (60-80  $\text{g kg}^{-1}$ ) at 64d (Fig. 4d).

244 The values of CaCl<sub>2</sub>-Si, CaCl<sub>2</sub>-Al and CaCl<sub>2</sub>-Ge were used to compute the values of the Al/Si and Ge/Si  
245 molar ratios at each extraction time (Table 3). The Al/Si ratio in the CaCl<sub>2</sub> extract (CaCl<sub>2</sub>-Al/Si) for the  
246 mixtures and aggregates was systematically largely below that for kaolinite at each extraction time. At 64d,  
247 the range of CaCl<sub>2</sub>-Al/Si was 0.02-0.10 and 0.018-0.03  $\text{mol mol}^{-1}$  for the mixtures and aggregates,  
248 respectively, compared to 0.15 for kaolinite. With increasing extraction time, the Ge/Si ratio in the CaCl<sub>2</sub>  
249 extract (CaCl<sub>2</sub>-Ge/Si) decreased from 3.13 to 0.27 for phytoliths, and from 21 to 1.8  $\mu\text{mol mol}^{-1}$  for kaolinite  
250 (Table 3). Note that the value of CaCl<sub>2</sub>-Ge/Si at 16h was 20.9 here against 24.7 in Li et al. (2022). The value  
251 of CaCl<sub>2</sub>-Ge/Si for the mixtures and aggregates was systematically below that for kaolinite at each extraction  
252 time. In the mixtures, CaCl<sub>2</sub>-Ge/Si ( $\mu\text{mol mol}^{-1}$ ) ranged from 5.25 to 10.07 at 16h; at 64d, it increased  
253 progressively from 0.11 to 0.62 with the increase in goethite concentration from 0 to 40  $\text{g kg}^{-1}$ , and reached  
254 1.28-1.42 at goethite concentrations of 60 and 80  $\text{g kg}^{-1}$ . In the aggregates, the range of CaCl<sub>2</sub>-Ge/Si was  
255 1.86-5.84 at 16h and 0.12-0.56  $\text{mmol mol}^{-1}$  at 64d, with no dependency on goethite concentration.

256

## 257 **4. Discussion**

### 258 **4.1. Aggregation reduced DOC release, while preserving kaolinite**

259 In the range of  $\text{pH}_{\text{CaCl}_2}$  values, the surface charge carried by kaolinite, phytoliths and OM was negative while  
260 it was positive for goethite (Li et al., 2022). These charge discrepancies enhanced colloidal interactions and

261 aggregation, as observed in tropical soils containing kaolinite and secondary Fe and Al oxides (Sanchez,  
262 2019; Van Wambeke, 1992), but also in a wide range of LAC soils worldwide (IUSS, 2015). The phytoliths  
263 were embedded in aggregates (Fig. 1a-e) in which kaolinite and goethite were intimately associated and  
264 homogeneously distributed in fine-sized domains (Fig. 1f-j). Yet TEM could not distinguish whether the  
265 association consisted of kaolinite particles covered with goethite or of small clusters regularly scattered in  
266 these domains (Cambier and Prost, 1981; Schwertmann, 1988). Such clusters can combine with OM and  
267 silt-sized components to form microaggregates (Dultz et al., 2018; Kaiser and Guggenberger, 2007; Kleber  
268 et al., 2015; Six et al., 2000; Six et al., 2002). The aggregates thus readily formed after a 32-day incubation  
269 (Fig. 1), as confirmed by the DOC release, used as a test assessing the process of aggregation. The DOC  
270 release was significantly reduced after aggregation regardless the concentration of goethite (Fig. 1k, Table  
271 S1). The reduction of DOC release by aggregation occurred even at low goethite content, but was largest in  
272 aggregates with highest goethite concentrations. This reduction implied a stabilization of OM in aggregates,  
273 as shown in various soil types with predominant 2:1 or 1:1 clay minerals (Six et al., 2002).

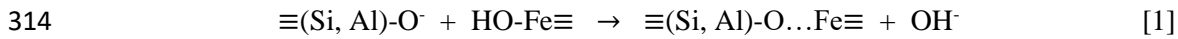
274 In the aggregates the ASi content, assumed to estimate the pool of biogenic silica (DeMaster, 1981), did not  
275 differ depending on goethite concentration as it ranged between 6 and 6.8 g kg<sup>-1</sup> (Table 2) whatever the  
276 concentration of goethite. Surprisingly, the ASi content was lowest in mixtures poor in goethite ( $\leq 10$  g kg<sup>-1</sup>)  
277 <sup>1</sup>) as it was 5.4-5.9 g kg<sup>-1</sup>, compared to ASi contents ranging from 7.6 to 9.2 g kg<sup>-1</sup> in mixtures with goethite  
278 content  $\geq 20$  g kg<sup>-1</sup>. Interestingly, the AAl content was significantly lower in aggregates than in mixtures,  
279 suggesting a protective effect of the aggregation process on kaolinite, which was the exclusive source of Al  
280 in our experimental model. Previous mineralogical investigations did not detect amorphous aluminosilicates  
281 in *Charentes kaolinite* (Yvon et al., 1982). Yet, they highlighted crystalline defects in kaolinite particles  
282 associated with a disorder increasing with decreasing particle size (Cases et al., 1982), likely linked to their  
283 Fe content (Mestdagh et al., 1982), and related to impurities in the crystal growth environment (Cases et al.,  
284 1982). These characteristics may have enhanced partial dissolution of fine-sized kaolinite particles in the  
285 alkaline extractant (Carroll-Webb and Walther, 1988; Devidal et al., 1997; Huertas et al., 1999; N'Guessan

286 et al., 2021). However, the very low AAl/ASi molar ratio, 0.05-0.12 in mixtures and 0.02-0.03 in aggregates,  
287 attested to a largely dominant dissolution of an amorphous silica phase attributed to phytoliths. The  
288 dissolution of quartz, as is possible under alkaline conditions (Dove, 1994), likely did not interfere with the  
289 assessment of ASi, since the procedure did not target crystalline forms of silica (De Master, 1981; Sauer et  
290 al., 2006; Meunier et al., 2014).

#### 291 **4.2. Goethite affected phytolith dissolution through aggregation and pH regulation**

292 The pH of the liquid phase during equilibration of the dilute CaCl<sub>2</sub> solution with the respective mixtures and  
293 aggregates can be regulated by various processes. These are potentially: deprotonation of hydroxyl groups  
294 in kaolinite and OM, Ca<sup>2+</sup> ↔ 2 H<sup>+</sup> ion exchange, H<sup>+</sup> uptake by goethite surface sites, H<sup>+</sup> consumption by  
295 kaolinite dissolution. The latter process was limited since the CaCl<sub>2</sub>-Al range was 1.4 × 10<sup>-6</sup>–1.9 × 10<sup>-4</sup>  
296 mol l<sup>-1</sup> in the mixtures and 0.8 × 10<sup>-6</sup>–1.0 × 10<sup>-4</sup> mol l<sup>-1</sup> in the aggregates (Table S2). Note that CaCl<sub>2</sub>-Al was  
297 nearly systematically and significantly smaller in the aggregates than in the mixtures (Table S2, Fig. S3):  
298 this suggests that aggregation protected kaolinite. Obviously, goethite played a role in regulating pH. The  
299 prolonged (64d) equilibration with the dilute CaCl<sub>2</sub> solution led to a significant increase in pH<sub>CaCl<sub>2</sub></sub> from 5.5  
300 to 7.5 with the increase in goethite concentration from 0 to 80 g kg<sup>-1</sup> (Fig. 2a). The tendency for soil pH to  
301 drift towards its pH<sub>IEP</sub> value (Uehara and Gillman, 1985) had long been recognized under the principle of  
302 “isoelectric weathering” (Mattson, 1932): the higher the pH<sub>IEP</sub>, the higher the soil pH, so that base-depleted,  
303 highly weathered soils rich in Al and Fe oxides can approach neutrality (Sanchez, 2019; Van Wambeke,  
304 1992). As the pH<sub>IEP</sub> value for goethite is 9.6, the increase in pH<sub>CaCl<sub>2</sub></sub> at 64d from 5.5 to 7.5 with increasing  
305 goethite content in mixtures ( $r = 0.93$ ,  $p < 0.01$ ) was consistent with the principle of isoelectric weathering,  
306 which involved here the release of protons by kaolinite and OM and their uptake by goethite. As reported  
307 by Arias et al. (1995), the coating of kaolinite surfaces by goethite particles changes the surface properties  
308 of kaolinite particles. Wei et al. (2014) showed that the intimate association of both minerals led to a higher  
309 pH<sub>IEP</sub> than in kaolinite-goethite mixture, probably because of the coating of kaolinite surfaces by fine  
310 goethite particles (Schwertmann, 1988). From their study, a higher pH<sub>CaCl<sub>2</sub></sub> was thus expected when

311 equilibrating the aggregates with dilute CaCl<sub>2</sub> compared to the mixtures, as observed here (Fig. 2). The  
312 mechanism involved is illustrated by the following reaction of deprotonated surface (Si, Al)-OH group of  
313 kaolinite with goethite hydroxyl (Wei et al., 2014):



315 Yet, in the absence of goethite, the higher pH<sub>CaCl<sub>2</sub></sub> in aggregate-0 than in mixture-0 (Fig. 1k) could be due  
316 to a higher retention of OM as discussed above, given that OM can be a proton donor.

317 In all mixtures and aggregates, the overall trend was that pH<sub>CaCl<sub>2</sub></sub> increased with increasing time up to 7.5-  
318 7.9 (Fig. 2), below the pH<sub>IEP</sub> of goethite (9.6). Thus, the role of goethite in pH stabilization was moderated  
319 by other constituents with lower pH<sub>IEP</sub>, as observed in soils (Sanchez, 2019), in which it may have a real  
320 effect at microsite level as illustrated here. In our experimental system, the increase in pH can have two  
321 potential consequences: (i) raising the sorption of aqueous Si on goethite surfaces (Hiemstra et al., 2007),  
322 thus removing Si from the liquid phase, (ii) enhancing phytolith dissolution (Fraysse et al., 2009), hence  
323 releasing Si in the liquid phase. Our data showed that phytolith dissolution took precedence over DSi  
324 adsorption. Indeed, the time evolution of pH<sub>CaCl<sub>2</sub></sub> (Fig.2a) and CaCl<sub>2</sub>-Si (Fig.3a) suggested a major impact  
325 of pH on the release of aqueous Si from mixtures, as regulated by goethite. At 64d, CaCl<sub>2</sub>-Si was almost  
326 doubled (335-575 mg kg<sup>-1</sup>) as pH increased from 5.5 to 7.5 with the increase in goethite content in the  
327 mixtures, whereas its range was much narrower in the aggregates (395-430 mg kg<sup>-1</sup>) under small pH  
328 variation (7.2-7.9) without dependence on goethite content (Fig. 2b, Fig. 3b). Given that aggregation  
329 significantly reduced the release of aqueous Si, both the aggregation process and pH had controlled the  
330 preservation of phytoliths and their dissolution, respectively. Fig. 5 illustrated this assessment: CaCl<sub>2</sub>-Si  
331 increased with increasing pH, but differently before and after aggregation. At pH values close to 5, Si release  
332 was similar in both the mixtures and aggregates. Above pH 5.5, CaCl<sub>2</sub>-Si increased less after aggregation  
333 with increasing pH, indicating a protective effect of the phytoliths within the aggregates, thus less phytolith  
334 dissolution and, consequently, less release of Si into the aqueous phase. From Fig. 5, using the linear  
335 regression equations at pH ≥ 6, CaCl<sub>2</sub>-Si was almost twice as small in the aggregates as in the mixtures.

336 To further assess the protection of phytoliths as induced by goethite-mediated aggregation, we defined its  
337 protective effect (*PrEf*) on the release of phytolithic Si using the CaCl<sub>2</sub>-Si values at 64<sup>th</sup> day as follows:

$$338 \quad PrEf = \frac{(\text{CaCl}_2\text{-Si in mixtures}) - (\text{CaCl}_2\text{-Si in aggregates})}{(\text{CaCl}_2\text{-Si in mixtures})} \times 100\% \quad [2]$$

339 As shown in Fig. 6, in the absence of goethite, *PrEf* was negative (-29%). In contrast, *PrEf* within the  
340 goethite-mediated aggregates raised from ~2% at goethite content of 10-20 g kg<sup>-1</sup> up to 20-30% with  
341 increasing goethite content. Thus, small amounts of goethite can have a significant effect on the protective  
342 action of aggregates on the preservation of phytoliths, hence delaying their dissolution, as noted through the  
343 release of both Si (Fig. 3) and Ge (Fig. 4). The release of Si and Ge in CaCl<sub>2</sub> extracts was strongly similar  
344 in two respects. Firstly, for the mixtures, both CaCl<sub>2</sub>-Ge and CaCl<sub>2</sub>-Si at 64d significantly increased with  
345 the increase in goethite content from 0 to 80 g kg<sup>-1</sup> as well as in pH from 5.5 to 7.5. Secondly, both the  
346 ranges of CaCl<sub>2</sub>-Ge and CaCl<sub>2</sub>-Si at 64d were much narrower in aggregates than in mixtures, without any  
347 dependence on goethite content. Thus, the fates of aqueous Ge and Si were strongly similar, and likely  
348 controlled by the same source.

349 Since the CaCl<sub>2</sub>-Si release from quartz and OM was negligible, the only sources of aqueous Si were  
350 phytoliths and kaolinite. Molar Ge/Si and Al/Si ratios can be used as geochemical proxies to trace the source  
351 of DSi. The Ge/Si ratio highly discriminates phytoliths from clay minerals (Blecker et al., 2007; Derry et  
352 al., 2005; White et al., 2012), particularly kaolinite (Lugolobi et al., 2010; Wiche et al., 2018). The Al/Si  
353 ratio sharply distinguishes phytoliths with Al/Si ~ 0 from kaolinite exhibiting Al/Si = 1.01 (Table 1). The  
354 time evolutions of CaCl<sub>2</sub>-Al/Si and -Ge/Si ratios for phytoliths and kaolinite (Table 3) were typical for these  
355 components (Li et al., 2022 and references therein). For mixtures and aggregates, the CaCl<sub>2</sub>-Al/Si and -  
356 Ge/Si values converged to identify the source of aqueous Si, namely phytoliths. Indeed, CaCl<sub>2</sub>-Al/Si and  
357 CaCl<sub>2</sub>-Ge/Si were systematically lower than those of kaolinite at each extraction time (Table 3), both for  
358 the mixtures and for the aggregates, but particularly for the latter. This was well illustrated in Fig. 7, showing  
359 the time evolution of the Al/Si and Ge/Si molar ratios in the CaCl<sub>2</sub> extracts from mixtures and aggregates.  
360 Clearly, both ratios decreased continuously to low values during prolonged equilibration with dilute CaCl<sub>2</sub>.

361 The Ge/Si values were very close to those of phytoliths, as evidenced from both hydroponic (Blecker et al.,  
362 2007) and field studies (White et al., 2012). In particular, phytoliths and aggregates were clearly  
363 discriminated from kaolinite during this equilibration, using both Al/Si and Ge/Si (Fig. 7b). Plotting our  
364 experimental data (Table S2) in the  $\text{Al}_2\text{O}_3\text{-SiO}_2\text{-H}_2\text{O}$  stability diagram (Fig. 8) further illustrated that  
365  $\text{H}_4\text{SiO}_4$  activity was controlled by phytoliths in both the mixtures and aggregates. Kaolinite was unstable  
366 because of low pH ( $\sim 3.8$ ) and relative desilication with ( $\text{H}_4\text{SiO}_4$ ) below  $10^{-3}$  M. In mixtures and aggregates,  
367 the stability of kaolinite increased during the  $\text{CaCl}_2$  extraction likely because of the increase in pH and silica  
368 activity due to phytolith dissolution. The combined use of Al/Si and Ge/Si molar ratios, pH and kinetic data  
369 thus allowed an unequivocal identification of DSi sources.

370 Our experimental data therefore validate our first research hypothesis. Indeed, the aggregation-induced  
371 protection of phytoliths has delayed their dissolution, thus reducing the release of DSi at low goethite  
372 concentrations ( $\geq 20$  g  $\text{kg}^{-1}$ ), most probably because of oxide fine size and high SSA. However, our data  
373 somehow invalidate our second hypothesis since the increase in pH did not cause identical behavior between  
374 mixtures and aggregates (Fig. 7). This indicates that the increase in pH, as driven by increasing goethite  
375 loading, did not lead to disaggregation and a subsequent increasing release of DSi caused by the liberation  
376 of phytoliths from microaggregates. Thus, the effect of increasing pH was likely to be to promote the  
377 dissolution of phytoliths that were not previously trapped in microaggregates, as their dissolution rate  
378 increases by about one order of magnitude from pH 5 to 8 (Frayssé et al., 2009). The poor or absent pH-  
379 induced disaggregation contrasts with earlier observations indicating disaggregation and clay dispersion  
380 upon liming highly weathered soils rich in Fe oxides (Bigham et al., 2002). However, it corroborates the  
381 stability of microaggregates observed in LAC soils with variable charge crystalline minerals as the soil pH  
382 drifts towards its  $\text{pH}_{\text{IEP}}$  (Goldberg, 1989). As predicted by the Derjaguin–Landau–Verwey–Overbeek  
383 (DLVO) theory, maximum aggregation should be achieved when surrounding pH approaches the particles  
384  $\text{pH}_{\text{IEP}}$  at which surface electrical potential is minimal (Goldberg, 1989; Guo et al., 2022). This would confirm

385 that, in our experimental scenario, the increase in pH had likely maintained or enhanced microaggregation,  
386 but promoted the dissolution of unembedded phytoliths.

### 387 **4.3. How does the Si sorption/desorption control DSi?**

388 Apart from phytolith and mineral dissolution, the sorption/desorption of DSi on secondary oxides was  
389 suggested to control DSi in soils (Cornelis et al., 2014; Meunier et al., 2018). Where soil phytoliths control  
390 DSi, as measured by  $\text{CaCl}_2\text{-Si}$ , this hypothesis is questioned since, here, phytolith dissolution took  
391 precedence over Si sorption on goethite. In our experimental scenario, goethite-mediated aggregation and  
392 pH regulation actually controlled the release of DSi, despite our experimental design did not consider  
393 competing solutes for goethite sorbing sites. Although oxide surface OH groups interact specifically with  
394  $\text{H}_4\text{SiO}_4$ , advocating DSi sorption/desorption in natural soils could then be moderated for three reasons. (i)  
395 In soils, various solutes compete strongly with  $\text{H}_4\text{SiO}_4$  to be adsorbed by oxides, notably organic and  
396 orthophosphate anions (Klotzbücher et al., 2020). (ii) The low reversibility of the Si sorption process may  
397 limit the additional sorption of aqueous Si (Haynes and Zou, 2020). (iii) The change in oxide surface  
398 composition due to inner sphere complexation shifts the  $\text{pH}_{\text{IEP}}$  value downwards (Anderson and Benjamin,  
399 1985; Kingston et al., 1972), which also reduces additional Si sorption (Bowden et al., 1973).

400

## 401 **5. Implications and conclusion**

402 From a geochemical perspective, soil processes impact the global fate of Si (Cornelis and Delvaux, 2016)  
403 since they control the fluxes of aqueous Si to the biosphere and hydrosphere, hence affecting the oceanic  
404 capacity to fix carbon by diatoms (Conley, 2002). In soils, phytoliths represent a major source of aqueous  
405 Si because of their relatively high dissolution rate (Frayse et al., 2009). Here we show that phytoliths can  
406 be preserved from dissolution by aggregation involving kaolinite and goethite, ubiquitous crystalline  
407 minerals with low charge and surface area. Such mineralogical pattern is typical for low activity clay (LAC)  
408 soils (Uehara and Gillman, 1985). LAC soils cover ~30% of the land surface at global scale and ~55% in  
409 the tropics. As the soil phytolith pool is a dominant, if not exclusive, contributor to the DSi pool in LAC

410 soils (Cornelis and Delvaux, 2016; Lucas et al., 1993; Meunier et al., 1999), phytolith trapping in  
411 microaggregates is therefore a worldwide soil process that can largely impact DSi fluxes in the global Si  
412 cycle. The role of the Fe oxide is highlighted here as it mediates aggregation under continuously oxic  
413 conditions, as they occur in well-aerated soils, which are largely dominant on earth (> 90% of global land  
414 surface). The protective effect of the aggregates on the preservation of phytoliths proves significant at low  
415 goethite content ( $\geq 2\%$ ). At common pH values of the soil solution (5-6), aggregation reduced Si release by  
416 2- to 3-fold, suggesting that phytolith preservation in soil aggregates can be more widespread than currently  
417 known, and likely more effective than Si adsorption on oxides for retaining Si. As already concluded earlier  
418 (Li et al., 2020; Li et al., 2022; Meunier et al., 2014; Vander Linden et al., 2021), the occurrence of two  
419 pools of phytoliths, namely fresh and stabilized, is also supported by our data. By using ubiquitous clay  
420 mineral and Fe oxide, we show that microaggregation can be a widespread soil process that contributes to  
421 build up the pool of stabilized phytoliths in soils, together with other processes such as, notably, the decrease  
422 in surrounding pH (Frayse et al., 2009), ageing (Liu et al., 2003; Puppe and Leue, 2018) and surface  
423 passivation (Koebernick et al., 2022). The latter process consists of the accumulation of Fe and C on the  
424 surfaces of phytoliths, which are thus protected from dissolution (Koebernick et al., 2022). As being  
425 enhanced by alternating redox conditions, this process involving Fe dynamics can occur in waterlogged  
426 soils with alternating redox conditions. It reduces the release of DSi from the “passivated” phytoliths by 3-  
427 fold (Koebernick et al., 2022), a reduction factor similar to that observed here after aggregation under oxic  
428 conditions, which are widely prevalent in well-aerated soils.

429 Clearly, laboratory studies (Koebernick et al., 2022; Li et al., 2022; present study) can show higher release  
430 rates of DSi from phytoliths than in natural soils. Since unsaturated flow through soil voids limits the amount  
431 of surface exposed to water in natural conditions, the rate of Si release would be significantly lower than  
432 predicted from our laboratory studies as demonstrated earlier for weathering, precipitation-dissolution and  
433 sorption-desorption processes (Stumm and Morgan, 1996). In addition, biological activity was not  
434 considered here, although it is crucial to further enhance microaggregation. Therefore, if the release of DSi

435 from phytoliths is so significantly reduced over short periods in laboratory conditions, as observed here, we  
436 can expect a higher impact of microaggregation on phytolith protection and DSi release reduction in natural  
437 soils. Thus, aggregation and above cited processes as well as specific properties of phytoliths (Cabanes et  
438 al, 2012; Puppe and Leue, 2018), can enhance the resilience of phytoliths in soils over Millenia (Monger  
439 and Kelly, 2002) and their use as paleo-indicators (Strömberg et al., 2018).

440

#### 441 **Declaration of Competing Interest**

442 The authors declare that they have no known competing financial interests or personal relationships that  
443 could have appeared to influence the work reported in this paper.

444

#### 445 **Acknowledgements**

446 Z. Li is supported by the Fonds National de la Recherche Scientifique (FNRS) of Belgium, as Chargé de  
447 recherches. This research was supported by FNRS, and Wallonie-Bruxelles International (WBI) for  
448 supporting the Partenariats Hubert Currien Tournesol (PHC Tournesol 2021). The authors warmly thank A.  
449 Iserentant, E. Devos, L. Monin and C. Givron for laboratory assistance in the analytical platform MOCA,  
450 UCLouvain, J.-F. Statsyns for surface analysis at IMCN-MOST, UCLouvain and L. Ryelandt for SEM/TEM  
451 analyses at IMMC-LACaMI, UCLouvain. We warmly thank the Associate Editor and the three anonymous  
452 reviewers for their critical analysis, which allowed us to improve the quality of our manuscript.

453

#### 454 **Appendix A. Supplementary material**

455 Supplementary material includes experimental results aimed at facilitating the understanding of data  
456 presented and discussed in the manuscript (MS).

457 Raw data illustrated in the MS figures are in a text-based numerical format at Tables S1 and S2: organic  
458 carbon budget and DOC release (Table S1), pH, concentrations ( $\text{mol l}^{-1}$ ) of  $\text{H}_4\text{SiO}_4$  and Al as well as of Ge  
459 ( $\mu\text{mol l}^{-1}$ ) in 0.01 M  $\text{CaCl}_2$  extracts as collected from 16 h to 64 d for phytoliths, quartz, kaolinite, and  
460 mixtures and aggregates (Table S2). Table S1 data are illustrated in the MS at Fig.1 while Table S2 data are  
461 used in all other figures, from Fig.2 to Fig.8 as well as in Table 3.

462 In addition, Fig. S1 presents the  $\text{Na}_2\text{CO}_3$ -dissolved Si and Al concentrations as measured in a kinetic  
463 extraction to estimate the contents of amorphous Si (ASi) and Al (AAl) used in Table 2 in the MS. Figure  
464 S1 reports on  $\text{CaCl}_2$ -extractable Si and Al that are used in the MS at Table 3, Fig. 7 and Fig. 8. Figure S3  
465 traces the temporal evolution of  $\text{CaCl}_2$  extractable Al as used in the MS at Fig. 7-8 and Table 3.

466

## 467 **References**

- 468 Anderson, P. R., Benjamin, M. M., 1985. Effect of silicon on the crystallization and adsorption properties  
469 of ferric oxides. *Environ. Sci. Technol.* 19, 1048-1053.
- 470 Arias M., Barral M. T., Diaz-Fierros F., 1995. Effects of iron and aluminium oxides on the colloidal and  
471 surface properties of kaolin. *Clays Clay Miner.* 43, 406-416.
- 472 Baalousha, M., 2009. Aggregation and disaggregation of iron oxide nanoparticles: influence of particle  
473 concentration, pH and natural organic matter. *Sci. Total Environ.* 407, 2093-2101.
- 474 Baalousha, M., Manciualea, A., Cumberland, S., Kendall, K., Lead, J.R., 2008. Aggregation and surface  
475 properties of iron oxide nanoparticles: influence of pH and natural organic matter. *Environ. Toxicol.*  
476 *Chem.* 27, 1875-1882.
- 477 Bartoli, F., 1983. The biogeochemical cycle of silicon in two temperate forest ecosystems. *Ecol. Bull.* 469-  
478 476.
- 479 Bigham, J., Fitzpatrick, R.W., Schulze, D., 2002. Iron oxides. *Soil mineralogy with environmental*  
480 *applications* 7, pp.323-366.
- 481 Blecker, S.W., King, S.L., Derry, L.A., Chadwick, O.A., Ippolito, J.A., Kelly, E.F., 2007. The ratio of  
482 germanium to silicon in plant phytoliths: quantification of biological discrimination under  
483 controlled experimental conditions. *Biogeochemistry.* 86, 189-199.
- 484 Bowden, J. W., Bolland, M. D. A., Posner, A. M., Quirk, J. P., 1973. Generalized model for anion and cation  
485 adsorption at oxide surfaces. *Nat. Phys. Sci.* 245, 81-83.
- 486 Cabanes, D., Gadot, Y., Cabanes, M., Finkelstein, I., Weiner, S., Shahack-Gross, R., 2012. Human impact  
487 around settlement sites: a phytolith and mineralogical study for assessing site boundaries, phytolith  
488 preservation, and implications for spatial reconstructions using plant remains. *J. Archaeol. Sci.* 39,  
489 2697-2705.
- 490 Cambier, P., Prost, R., 1981. Etude des associations argile-oxyde: organisation des constituants d'un  
491 matériau ferrallitique. *Agronomie.* 1, 713-722.
- 492 Carroll-Webb, S. A., Walther, J. V., 1988. A surface complex reaction model for the pH-dependence of  
493 corundum and kaolinite dissolution rates. *Geochim. Cosmochim. Acta.* 52, 2609-2623.

494 Cases, J.-M., Villiéras, F., Michot, L., 2000. Les phénomènes d'adsorption, d'échange ou de rétention à  
495 l'interface solide-solution aqueuse. 1. Connaissance des propriétés structurales, texturales et  
496 superficielles des solides. C. R. Acad. Sci., Ser. 2 Earth Planet. Sci. 331, 763–773.

497 Cases, J.M., Liétard, O., Yvon, J., Delon, J.F., 1982. Etude des propriétés cristallographiques,  
498 morphologiques, superficielles de kaolinites désordonnées. Bull. Mineral. 105, 439-455.

499 Cate Jr, R. B., Nelson, L. A., 1971. A simple statistical procedure for partitioning soil test correlation data  
500 into two classes. Soil Sci. Soc. Am. J. 35, 658–660.

501 Chao, T., Sanzolone, R., 1992. Decomposition techniques. J. Geochem. Explor. 44, 65-106.

502 Chenu, C., Cosentino, D., 2011. Microbial Regulation of Soil Structural Dynamics, in Ritz, K., Young, I.  
503 (eds.): The Architecture and Biology of Soils: Life in Inner Space. CAB International, Wallingford,  
504 UK, pp. 37–70.

505 Conley, D. J., 2002. Terrestrial ecosystems and the global biogeochemical silica cycle. Glob. Biogeochem.  
506 Cycles. 16, 1121.

507 Conley, D. J., Carey, J. C., 2015. Silica cycling over geologic time. Nat. Geosci. 8, 431-432.

508 Cornelis, J. T., Delvaux, B., 2016. Soil processes drive the biological silicon feedback loop. Funct. Ecol.  
509 30, 1298-1310.

510 Cornelis, J. T., Dumon, M., Tolossa, A. R., Delvaux, B., Deckers, J., Van Ranst, E., 2014. The effect of  
511 pedological conditions on the sources and sinks of silicon in the Vertic Planosols in south-western  
512 Ethiopia. Catena. 112, 131-138.

513 Cornell, R., Schwertmann, U., 1996. The Iron Oxides: Structures, Properties, Reactions, Occurrences and  
514 Uses. VCH Verlagsgesellschaft GMBH, Weinheim, Germany, pp.533-559.

515 Coskun, D., Deshmukh, R., Sonah, H., Menzies, J.G., Reynolds, O., Ma, J.F., Kronzucker, H.J. Bélanger,  
516 R.R., 2019. The controversies of silicon's role in plant biology. New Phytol. 221, 67-85.

517 De Gryze, S., Six, J., Merckx, R., 2006. Quantifying water-stable soil aggregate turnover and its implication  
518 for soil organic matter dynamics in a model study. Eur. J. Soil Sci. 57, 693–707.

519 Delineau, T., Allard, T., Muller, J.P., Barres, O., Yvon, J., Cases, J.M., 1994. FTIR reflectance vs. EPR  
520 studies of structural iron in kaolinites. Clays Clay Miner. 42, 308-320.

521 Demangeat, E., Pédrot, M., Dia, A., Bouhnik-le-Coz, M., Grasset, F., Hanna, K., Kamagate, M. and Cabello-  
522 Hurtado, F., 2018. Colloidal and chemical stabilities of iron oxide nanoparticles in aqueous  
523 solutions: the interplay of structural, chemical and environmental drivers. Environ. Sci. Nano. 5,  
524 992-1001.

525 DeMaster, D. J., 1981. The supply and accumulation of silica in the marine environment. Geochim.  
526 Cosmochim. Acta. 45, 1715-1732.

527 Deneff, K., Six, J., Merckx, R., Paustian, K., 2002. Short-term effects of biological and physical forces on  
528 aggregate formation in soils with different clay mineralogy. Plant Soil. 246, 185-200.

529 Deng, Y., Dixon, J.B., 2002. Soil organic matter and organic-mineral interactions. Soil mineralogy with  
530 environmental applications. 7, pp.69-107.

531 Derry, L.A., Kurtz, A.C., Ziegler, K., Chadwick, O.A., 2005. Biological control of terrestrial silica cycling  
532 and export fluxes to watersheds. Nature. 433, 728-731.

533 Deshpande, T. L., Greenland, D. J., Quirk, J. P., 1964. Role of iron oxides in the bonding of soil particles.  
534 Nature. 201, 107-108.

535 Devidal, J.L., Schott, J., Dandurand, J.L., 1997. An experimental study of kaolinite dissolution and  
536 precipitation kinetics as a function of chemical affinity and solution composition at 150 C, 40 bars,  
537 and pH 2, 6.8, and 7.8. Geochim. Cosmochim. Acta. 61, 5165-5186.

538 Di Iorio, E., Circelli, L., Angelico, R., Torrent, J., Tan, W., Colombo, C., 2022. Environmental implications  
539 of interaction between humic substances and iron oxide nanoparticles: A review. Chemosphere.  
540 135172.

541 Dove, P. M., 1994. The dissolution kinetics of quartz in sodium chloride solutions at 25 degrees to 300  
542 degrees C. Am. J. Sci. 294, 665-712.

543 Dultz, S., Steinke, H., Mikutta, R., Woche, S.K., Guggenberger, G., 2018. Impact of organic matter types  
544 on surface charge and aggregation of goethite. *Colloids Surf. A Physicochem. Eng. Asp.* 554, 156-  
545 168.

546 Epstein, E., 1994. The anomaly of silicon in plant biology. *PNAS.* 91, 11-17.

547 Erhart, H., 1963. Sur le cycle de la silice hydratée dans la biosphère. *CR Acad. Sci. Paris.* 256, 3731-3734.

548 Filimonova, S., Kaufhold, S., Wagner, F.E., Häusler, W., Kögel-Knabner, I., 2016. The role of allophane  
549 nano-structure and Fe oxide speciation for hosting soil organic matter in an allophanic Andosol.  
550 *Geochim. Cosmochim. Acta.* 180, 284-302.

551 Fraysse, F., Pokrovsky, O.S., Schott, J., Meunier, J.D., 2009. Surface chemistry and reactivity of plant  
552 phytoliths in aqueous solutions. *Chem. Geol.* 258, 197-206.

553 Garrels, R.M., Christ, C.L., 1965. *Solutions, Minerals and Equilibria.* W. H. Freeman, San Francisco.

554 Goldberg, S., 1989. Interaction of aluminum and iron oxides and clay minerals and their effect on soil  
555 physical properties: a review. *Commun. Soil Sci. Plant Anal.* 20, 1181-1207.

556 Guo, Y., Tang, N., Guo, J., Lu, L., Li, N., Hu, T., Zhu, Z., Gao, X., Li, X., Jiang, L., Liang, J., 2022. The  
557 aggregation of natural inorganic colloids in aqueous environment: A review. *Chemosphere.* 136805.

558 Haynes, R. J., Zhou, Y. F., 2020. Silicate sorption and desorption by a Si-deficient soil—Effects of pH and  
559 period of contact. *Geoderma.* 365, 114204.

560 Haysom, M., Chapman, L., 1975. Some aspects of the calcium silicate trials at Mackay. *Proc. Conf. Qld*  
561 *Soc. Sugar Cane Technol.* 42, 117–122.

562 Hiemstra, T., Barnett, M.O., van Riemsdijk, W.H., 2007. Interaction of silicic acid with goethite. *J. Colloid*  
563 *Interface Sci.* 310, 8-17.

564 Hodson, M.J., White, P.J., Mead, A., Broadley, M.R., 2005. Phylogenetic variation in the silicon  
565 composition of plants. *Ann. Bot.* 96, 1027-1046.

566 Houba, V.J.G., Temminghoff, E.J.M., Gaikhorst, G.A., Van Vark, W., 2000. Soil analysis procedures using  
567 0.01 M calcium chloride as extraction reagent. *Commun. Soil Sci. Plant Anal.* 31, 1299-1396.

568 Huertas, F.J., Chou, L., Wollast, R., 1999. Mechanism of kaolinite dissolution at room temperature and  
569 pressure Part II: Kinetic study. *Geochim. Cosmochim. Acta.* 63, 3261-3275.

570 ICPT., 2019. International code for phytolith nomenclature (ICPN) 2.0. *Ann. Bot.* 124, 189-199.

571 IUSS., 2015. World Reference Base for Soil Resources 2014, update 2015. International Soil Classification  
572 System for Naming Soils and Creating Legends for Soil Maps. FAO, Rome, Italy.

573 Kaiser, K., Guggenberger, G., 2007. Sorptive stabilization of organic matter by microporous goethite:  
574 sorption into small pores vs. surface complexation. *Eur. J. Soil Sci.* 58, 45-59.

575 Karathanasis, A., 2002. Mineral equilibria in environmental soil systems. *Soil mineralogy with*  
576 *environmental applications.* 7, pp.109-151.

577 Kelly, E., 1990. Methods for extracting opal phytoliths from soil and plant material: Workshop on biotic  
578 indicators of global change. University of Washington.

579 Kingston, F. J., Posner, A. M., Quirk, J. T., 1972. Anion adsorption by goethite and gibbsite: I. The role of  
580 the proton in determining adsorption envelopes. *J. Soil Sci.* 23, 177-192.

581 Kleber, M., Eusterhues, K., Keiluweit, M., Mikutta, C., Mikutta, R., Nico, P.S., 2015. Mineral–organic  
582 associations: formation, properties, and relevance in soil environments. *Adv. Agron.* 130, pp.1-140.

583 Klotzbücher, T., Treptow, C., Kaiser, K., Klotzbücher, A., Mikutta, R., 2020. Sorption competition with  
584 natural organic matter as mechanism controlling silicon mobility in soil. *Sci Rep.* 10, 1-11.

585 Koebernick, N., Mikutta, R., Kaiser, K., Klotzbücher, A., Klotzbücher, T., 2022. Redox-dependent surface  
586 passivation reduces phytolith solubility. *Geoderma.* 428, 116158.

587 Koning, E., Epping, E., Van Raaphorst, W., 2002. Determining biogenic silica in marine samples by tracking  
588 silicate and aluminium concentrations in alkaline leaching solutions. *Aquat. Geochem.* 8, 37-67.

589 Li, Z., de Tombeur, F., Vander Linden, C., Cornelis, J.T., Delvaux, B., 2020. Soil microaggregates store  
590 phytoliths in a sandy loam. *Geoderma.* 360, 114037.

591 Li, Z., Meunier, J.D., Delvaux, B., 2022. Aggregation reduces the release of bioavailable silicon from  
592 allophane and phytolith. *Geochim. Cosmochim. Acta.* 325, 87-105.

593 Li, Z., Unzué-Belmonte, D., Cornelis, J.T., Linden, C.V., Struyf, E., Ronsse, F., Delvaux, B., 2019. Effects  
594 of phytolith rice-straw biochar, soil buffering capacity and pH on silicon bioavailability. *Plant*  
595 *Soil.* 438, 187-203.

596 Lindsay, W. L., 1979. *Chemical equilibria in soils.* John Wiley and Sons Ltd, Chichester, Sussex.

597 Liu, H., Meunier, J. D., Grauby, O., Labille, J., Alexandre, A., Barboni, D., 2023. Dissolution does not affect  
598 grass phytolith assemblages. *Palaeogeogr. Palaeoclimatol. Palaeoecol.* 610, 111345.

599 Lucas, Y., Luizão, F.J., Chauvel, A., Rouiller, J., Nahon, D., 1993. The relation between biological activity  
600 of the rain forest and mineral composition of soils. *Science.* 260, 521-523.

601 Lugolobi, F., Kurtz, A.C. and Derry, L.A., 2010. Germanium-silicon fractionation in a tropical, granitic  
602 weathering environment. *Geochim. Cosmochim. Acta.* 74, 1294–1308.

603 Mattson, S., 1932. The laws of soil colloidal behavior: IX Amphoteric reactions and isoelectric weathering.  
604 *Soil Science.* 34, 209.

605 Mestdagh, M.M., Herbillon, A.J., Rodrique, L., Rouxhet, P., 1982. Evaluation of the Role of Structural, Iron  
606 On Kaolinite Crystallinity. *Bull. Mineral.* 105, 457.

607 Meunier, J. D., Colin, F., Alarcon, C., 1999. Biogenic silica storage in soils. *Geology.* 27, 835-838.

608 Meunier, J. D., Sandhya, K., Prakash, N. B., Borschneck, D., Dussouillez, P., 2018. pH as a proxy for  
609 estimating plant-available Si? A case study in rice fields in Karnataka (South India). *Plant Soil.* 432,  
610 143-155.

611 Meunier, J.D., Cornu, S., Keller, C., Barboni, D., 2022. The role of silicon in the supply of terrestrial  
612 ecosystem services. *Environ. Chem. Lett.* 20, 2109–2121.

613 Meunier, J.D., Keller, C., Guntzer, F., Riotte, J., Braun, J.J., Anupama, K., 2014. Assessment of the 1%  
614 Na<sub>2</sub>CO<sub>3</sub> technique to quantify the phytolith pool. *Geoderma.* 216, 30-35.

615 Monger, C., Kelly, E., 2002. Silica minerals. *Soil mineralogy with environmental applications.* Ed. Dixon  
616 JB, Schulze DG SSSA Book Series 7. Soil Science Society of America. Madison, WI, USA, pp.611-  
617 635.

618 N'Guessan, N.E., Joussein, E., Courtin-Nomade, A., Paineau, E., Soubrand, M., Grauby, O., Robin, V.,  
619 Cristina, C.D., Vantelon, D., Launois, P., Fondanèche, P., 2021. Role of cations on the dissolution  
620 mechanism of kaolinite in high alkaline media. *Appl. Clay Sci.* 205, 106037.

621 Oades. J.M., 1984. Soil organic matter and structural stability: mechanisms and implications for  
622 management. *Plant Soil.* 76, 319-337.

623 Puppe, D., 2020. Review on protozoic silica and its role in silicon cycling. *Geoderma.* 365, 114224.

624 Puppe, D., Leue, M., 2018. Physicochemical surface properties of different biogenic silicon structures:  
625 Results from spectroscopic and microscopic analyses of protistic and phytogenic silica. *Geoderma.*  
626 330, 212-220.

627 Saccone, L., Conley, D.J., Sauer, D., 2006. Methodologies for amorphous silica analysis. *J. Geochem.*  
628 *Explor.* 88, 235-238.

629 Sanchez, P. A., 2019. *Properties and Management of Soils in the Tropics.* Cambridge University Press.

630 Sauer, D., Saccone, L., Conley, D.J., Herrmann, L., Sommer, M., 2006. Review of methodologies for  
631 extracting plant-available and amorphous Si from soils and aquatic sediments. *Biogeochemistry.*  
632 80, 89-108.

633 Schwertmann, U., 1988. Some properties of soil and synthetic iron oxides. *In Iron in soils and clay minerals*  
634 Springer, Dordrecht, pp.203-250.

635 Segoli, M., De Gryze, S., Dou, F., Lee, J., Post, W.M., Deneff, K., Six, J., 2013. AggModel: A soil organic  
636 matter model with measurable pools for use in incubation studies. *Ecol. Modell.* 263, 1–9

637 Six, J., Bossuyt, H., Degryze, S., Deneff, K., 2004. A history of research on the link between (micro)  
638 aggregates, soil biota, and soil organic matter dynamics. *Soil Till Res.* 79, 7-31.

639 Six, J., Conant, R.T., Paul, E.A., Paustian, K., 2002. Stabilization mechanisms of soil organic matter:  
640 implications for C-saturation of soils. *Plant Soil.* 24, 155-176.

641 Six, J.A.E.T., Elliott, E.T., Paustian, K., 2000. Soil macroaggregate turnover and microaggregate formation:  
642 a mechanism for C sequestration under no-tillage agriculture. *Soil Biol. Biochem.* 32, 2099-210.

643 Strömberg, C.A., Dunn, R.E., Crifò, C., Harris, E.B., 2018. Phytoliths in paleoecology: analytical  
644 considerations, current use, and future directions. In *Methods in Paleoecology*. Springer, Cham, pp.  
645 235–287.

646 Stumm, W., Morgan, J.J., 1996. *Aquatic chemistry: chemical equilibria and rates in natural waters*. John  
647 Wiley & Sons, Inc. New York.

648 Totsche, K.U., Amelung, W., Gerzabek, M.H., Guggenberger, G., Klumpp, E., Knief, C., Lehdorff, E.,  
649 Mikutta, R., Peth, S., Prechtel, A., Ray, N., 2018. Microaggregates in soils. *J. Plant. Nutr. Soil Sci.*  
650 181, 104-136.

651 Uehara, G., Gillman, G., 1985. *The mineralogy, chemistry, and physics of tropical soils with variable charge*  
652 *clays*. Westview Press Inc.

653 Van Wambeke, A. R., 1992. *Soils of the tropics: properties and appraisal*. McGraw Hill.

654 Vander Linden, C., Li, Z., Iserentant, A., Van Ranst, E., de Tombeur, F., Delvaux, B., 2021. Rainfall is the  
655 major driver of plant Si availability in perudic gibbsitic Andosols. *Geoderma*. 404, 115295.

656 Wei, S., Tan, W., Liu, F., Zhao, W., Weng, L., 2014. Surface properties and phosphate adsorption of binary  
657 systems containing goethite and kaolinite. *Geoderma*. 213, 478-484.

658 Wei, S., Tan, W., Zhao, W., Yu, Y., Liu, F., Koopal, L.K., 2012. Microstructure, interaction mechanisms,  
659 and stability of binary systems containing goethite and kaolinite. *Soil Sci. Soc. Am. J.* 76, 389-398.

660 West, S.L., White, G.N., Deng, Y., McInnes, K.J., Juo, A.S.R., Dixon, J.B., 2004. Kaolinite, halloysite, and  
661 iron oxide influence on physical behavior of formulated soils. *Soil Sci. Soc. Am. J.* 68, 1452-1460.

662 White, A.F., Vivit, D.V., Schulz, M.S., Bullen, T.D., Evett, R.R., Agarwal, J., 2012. Biogenic and  
663 pedogenic controls on Si distributions and cycling in grasslands of the Santa Cruz soil  
664 chronosequence, California. *Geochim. Cosmochim. Acta*. 94, 72-94.

665 White, G. N., Dixon, J. B., 2002. Kaolin–serpentine minerals. *Soil Mineral. Environ. Appl.* 7, pp.389–414.

666 Wiche, O., Székely, B., Moschner, C., Heilmeyer, H., 2018. Germanium in the soil-plant system – a review.  
667 *Environ. Sci. Pollut. Res.* 25, 31938-31956.

668 Yvon, J., Liétard, O., Cases, J.M., Delon, J.F., 1982. *Minéralogie des argiles kaoliniques des Charentes*.  
669 *Bull. Mineral.* 105, 431-437.

670 Zuo, X., Lu, H., Jiang, L., Zhang, J., Yang, X., Huan, X., He, K., Wang, C., Wu, N., 2017. Dating rice  
671 remains through phytolith carbon-14 study reveals domestication at the beginning of the Holocene.  
672 *PNAS*. 114, 6486-6491.